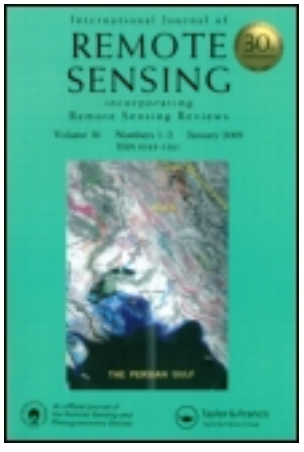

International Journal of Remote Sensing

Publication details, including instructions for authors and subscription information:
http://www.tandfonline.com/loi/tres20

Derivation of land surface temperatures from MODIS data using the general split-window technique

C. O. Mito [a b], G. Laneve [a], M. M. Castronuovo [a] & C. Ulivieri [b]

[a] Department of Physics, University of Nairobi, Nairobi, Kenya

[b] University of Rome 'La Sapienza', Via Salaria 851, 00138 Rome, Italy

Available online: 22 Feb 2007

To cite this article: C. O. Mito, G. Laneve, M. M. Castronuovo & C. Ulivieri (2006): Derivation of land surface temperatures from MODIS data using the general split-window technique, International Journal of Remote Sensing, 27:12, 2541-2552

To link to this article: http://dx.doi.org/10.1080/01431160500502579

International Journal of Remote Sensing
Vol. 27, No. 12, 20 June 2006, 2541–2552

Taylor & Francis
Taylor & Francis Group

Derivation of land surface temperatures from MODIS data using the general split-window technique

C. O. MITO*†‡, G. LANEVE‡, M. M. CASTRONUOVO‡ and C. ULIVIERI‡
†Department of Physics, University of Nairobi, PO Box 30197, Nairobi, Kenya
‡University of Rome 'La Sapienza', Via Salaria 851, 00138 Rome, Italy

(*Received 14 April 2004; in final form 22 November 2005*)

Fast Atmospheric Signature Code (FASCODE), a line-by-line radiative transfer programme, was used to simulate Moderate Resolution Imaging Spectroradiometer (MODIS) data at wavelengths 11.03 and 12.02 μm to ascertain how accurately the land surface temperature (LST) can be inferred, by the split-window technique (SWT), for a wide range of atmospheric and terrestrial conditions. The approach starts from the Ulivieri algorithm, originally applied to Advanced Very High Resolution Radiometer (AVHRR) channels 4 and 5. This algorithm proved to be very accurate compared to several others and takes into account the atmospheric effects, in particular the water vapour column (WVC) amount and a non-unitary surface emissivity. Extended simulations allowed the determination of new coefficients of this algorithm appropriate to MODIS bands 31 and 32, using different atmospheric conditions. The algorithm was also improved by removing some of the hypothesis on which its original expression was based. This led to the addition of a new corrective term that took into account the interdependence between water vapour and non-unitary emissivity values and their effects on the retrieved surface temperature. The LST products were validated within 1 K with *in situ* LSTs in 11 cases.

1. Introduction

Land surface temperature (LST) is an important factor in the control of most physical, chemical and biological processes of the Earth. Knowledge of the LST is necessary for many environmental studies and management activities of the Earth's resources (Li and Becker 1993). The extensive application and significant importance of temperature in environmental studies and management is the main force driving the study of LST in remote sensing. Significant progress has been made in estimation of land surface emissivity and temperature from airborne thermal infrared (TIR) data. A technique to estimate the surface temperature based on an assumed constant emissivity in one channel and previously determined atmospheric parameters was developed (Kahle *et al.* 1980). A variety of split-window techniques (SWTs) have been developed to retrieve sea surface temperature (SST) and LST from National Oceanic and Atmospheric Administration (NOAA) AVHRR data. The split-window LST method corrects the atmospheric effects based on the differential absorption in infrared bands (Price 1984, Ulivieri and Cannizzaro 1985a, Becker 1987, Wan and Dozier 1989, Becker and Li 1990, Sobrino *et al.* 1991, Vidal 1991, Kerr *et al.* 1992, Ottle and Stoll 1993, Prata 1994, Ulivieri *et al.* 1994, Wan and

*Corresponding author. Email: collins@uonbi.ac.ke

International Journal of Remote Sensing
ISSN 0143-1161 print/ISSN 1366-5901 online © 2006 Taylor & Francis
http://www.tandf.co.uk/journals
DOI: 10.1080/01431160500502579

Dozier 1996). The most popular form of the split-window algorithm is $T_s = T_4 + A(T_4 - T_5) + B$, where T_s is the LST, T_4 and T_5 are the brightness temperatures of AVHRR channels 4 and 5, and A and B are coefficients related to atmospheric effects, viewing angle and ground emissivity. A major problem in using split-window LST methods is that we need to know the surface emissivities in the bands better than 0.01. It seems possible to have such knowledge of the emissivities for certain types of land cover, such as lake surfaces, snow/ice, dense evergreen canopies, and some soils. For land cover with variable emissivities, especially in semi-arid and arid areas, it is almost impossible to estimate two band-averaged emissivities to such accuracy. Therefore, it is necessary to develop algorithms to retrieve LST without prior knowledge of emissivities or algorithms that retrieve LST and surface emissivity simultaneously (Wan and Li 1997).

The retrieval of surface temperatures from AVHRR measurements over land has shown that the problem is well understood from a theoretical viewpoint. Because of inherent sensor noise and the lack of adequate data on the atmospheric state as well as on the surface emissivity, however, AVHRR-derived LSTs are currently subject to uncertainties.

This situation may improve substantially with the availability of new instruments with better performance for both ground observation and atmosphere sounding. Such instruments should preferably all be mounted on the same platform to ensure contemporary measurements. Some of these platforms and sensors capable of such high quality measurements have recently been designed; such as, for example, the satellite series in the frame of the Earth Observing System (EOS) of the National Aeronautics and Space Administration (NASA), the Meteosat Second Generation (MSG) satellite, and the Environmental Satellite (ENVISAT) platform of the European Space Agency (ESA).

MODIS is an EOS instrument that serves as the keystone (Salomonson *et al.* 1989) for global studies of atmosphere (King *et al.* 1992), land (Running *et al.* 1994) and ocean processes. It scans $\pm 55^\circ$ from the nadir in 36 bands, with bands 1–19 and band 26 in the visible and near-infrared (NIR) range, and the remaining bands in the TIR from 3 to 15 μm. The specifications of MODIS bands have been published (Wan and Li 1997).

The bands in transparent atmospheric windows are designed for the remote sensing of surface properties. Other bands are mainly for atmospheric studies. MODIS provides images of daylight reflection and day/night emission of the Earth, repeating global coverage every 1–2 days. It uses 12 bits for quantization in all bands. The TIR bands have an Instantaneous Field-Of-View (IFOV) of 1 km at nadir. MODIS is particularly useful because of its global coverage, radiometric resolution and dynamic ranges, and accurate calibration in multiple TIR bands (better than 1% absolute) designed for retrieval of SST, LST and atmospheric properties.

Specifically, all atmospheric channels of MODIS are used to retrieve atmospheric temperature and water vapour profiles. Band 26 detects cirrus clouds and TIR bands 20, 22, 23, 29 and 31–33 correct atmospheric effects and retrieve surface emissivity and temperature. Multiple bands in the mid-infrared range provide, for the first time, corrections for solar radiation in daytime LST estimations using mid-infrared data. Taking advantage of the seven TIR bands of the MODIS instrument, a day–night algorithm has been proposed based on pairs of co-located measurements to retrieve simultaneously the surface temperature and the spectral emissivity without a knowledge of the atmospheric temperature and water vapour column (WVC) amount (Wan and Dozier 1996, Wan and Li 1997, Wan *et al.* 2002). Wan

and Li (1997) developed a physics-based LST algorithm for simultaneously retrieving surface band-averaged emissivities and temperatures from day/night pairs of MODIS data in seven TIR bands. Their LST algorithm was tested with simulated MODIS data for 80 sets of band-averaged emissivities calculated from published spectral data of terrestrial materials in wide ranges of atmospheric and surface temperature conditions. The results of their comprehensive sensitivity and error analysis to evaluate the performance of the new LST algorithm and its dependence on variations in surface emissivity and temperature, upon atmospheric conditions, as well as the noise-equivalent temperature difference (NEΔT) and calibration accuracy specifications of the MODIS instrument are published in the same paper. As a constraint, this algorithm has augmented probability of no cloud-free conditions because retrieval is based on two images. This obviously reduces the portion of Earth areas suitable for its application.

Figure 1 shows the absorption corresponding to water vapour (H_2O), ozone (O_3) and carbon dioxide (CO_2) in the 750–1050 cm^{-1} spectral range together with the relative response functions of AVHRR channels 4 (Ch 4) and 5 (Ch 5) and MODIS bands 31 (Ba 31) and 32 (Ba 32). These calculations were performed for a typical scenario for the equatorial region, using the PcLnWin Radiative Transfer (RT) programme from Ontar Corporation (http//www.ontar.com/products.html) in a clear sky (23 km visibility), with total water vapour content of 4.2 g cm^{-2} at nadir.

It is evident how MODIS bands 31 and 32 reproduce well the AVHRR channels 4 and 5, which have been used in the past to develop SWT and adapted SWT algorithms. The spectral ranges (figure 1) of the two bands are closer to each other compared to AVHRR and therefore the usual assumption of linearization of the Planck function is more justified for any SWT algorithm development. This assumption requires that the measurements be made in two spectral ranges close to each other, such that one of the measured radiances may be expressed as a linear function of the other.

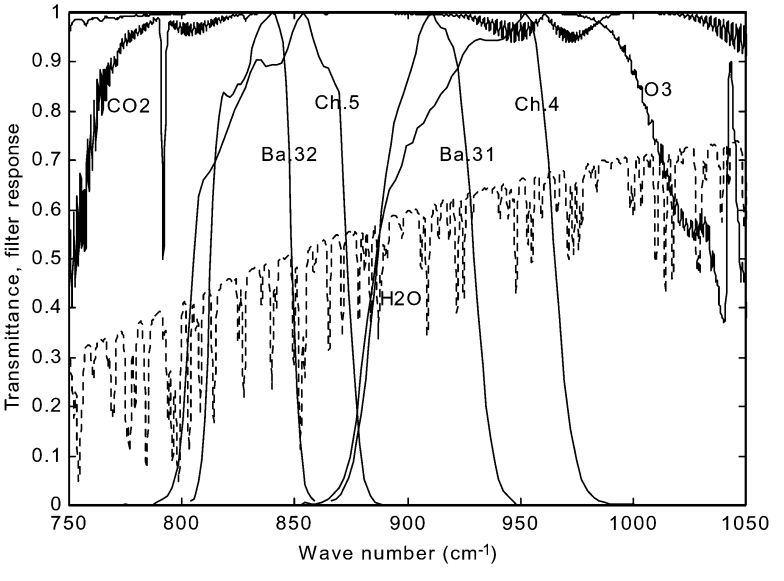

Figure 1. Absorption of the atmospheric constituents and filter response of AVHRR/2 and MODIS.

2. Theoretical basis of the algorithm

When the surface reflectance $\rho_i = 1 - \varepsilon_i$ is not negligible, the total radiance I_i emerging at the top of a nonscattering cloud-free atmosphere is given, in any selected radiometric band centred in i, by the relationship:

$$I_i = \varepsilon_i \tau_i B_i(T_s) + \overline{B_i}(1-\tau_i) + (1-\varepsilon_i)(1-\tau_i)\tau_i \overline{\overline{B_i}} \quad (1)$$

where B_i is the Planck intensity (watt cm^{-2} sr^{-1} μm^{-1}), T_S is the surface temperature (K), ε_i the spectral surface emittance, τ_i the total atmospheric spectral transmittance, and $\overline{B_i}$ and $\overline{\overline{B_i}}$ the upwelling and downwelling atmospheric mean radiance.

To make practical use of multitemporal and multichannel data, we need to simplify equation (1) by using some realistic assumptions about the surface optical properties (Wan and Li 1997). We assume that (a) the surface emissivity changes with vegetation coverage and surface moisture content. However, it does not significantly change in several days unless rain and/or snow occur during a short period of time – particularly for bare soils in arid and semi-arid environments (for which the surface of the ground is normally dry) (Kerr *et al.* 1992). We also assume that (b) there are quite strong spectral variations in surface reflectance for most terrestrial materials in the wavelength range 3.5–4.2 μm (Salisbury and D'Aria 1994) but their Bidirectional Reflectance Distribution Function (BRDF) anisotropic factor in this wavelength range has very small variations in the order of 2% (Snyder and Wan 1996, Snyder *et al.* 1997). It is therefore appropriate to assume that a single BRDF anisotropic factor can be used for the surface-reflected solar beam in MODIS bands 20, 22 and 23 located in this wavelength range (Wan and Li 1997). This anisotropic factor is defined by the ratio of the surface-reflected solar beam at the view direction of the MODIS sensor to the radiance that would have resulted if the surface reflected isotropically (such a surface is called a Lambertian surface). Atmospheric radiative transfer simulations show that (Wan and Li 1997), in clear-sky conditions, the surface-reflected diffuse solar irradiance term in the TIR range and the surface-reflected atmospheric downward thermal irradiance term are smaller than surface thermal emission. Therefore the Lambertian approximation of the surface reflection does not introduce a significant error in the 3–14 μm TIR region.

Although there is ample evidence that the emissivities of land surfaces such as soils, sands and vegetation canopies vary with viewing angle, there are few such spectral, angular emissivity data available. We therefore assume that land surfaces are Lambertian, so emissivity is independent of the viewing angle. This approximation is usually acceptable for viewing angles up to about 40° from nadir. We can therefore link the surface spectral emissivity ε_i to the surface spectral reflectance ρ_i by $\rho_i = 1 - \varepsilon_i$ according to Kirchoff's law.

Equation (1) may be rewritten in a more convenient form by introducing the quantities:

$$\begin{cases} E_i = \varepsilon_i \tau_i \\ A_i = [1 + (1-\varepsilon_i)\tau_i z_i](1-\tau_i) \end{cases} \quad (2)$$

where $z_i = \overline{\overline{B_i}} \Big/ \overline{B_i}$. Substituting these expressions in equation (1), the equation for the remotely sensed radiance at the satellite sensor becomes:

$$I_i = E_i B_i(T_s) + A_i \overline{B}_i \quad (3)$$

The General Split-Window Technique (GSWT) is based on a suitable combination of the relations derived from equation (3) for two adjacent spectral channels. This may be achieved by expanding equation (3) around a reference temperature. However, following McMillin (1975, 1980), it is considerably more accurate, especially when the wavelengths are close to each other, to expand the Planck function at a reference wavelength. Adapting McMillin's results to the formalism of equation (3), the following system is found:

$$\begin{cases} I_1 = E_1 B_1(T_s) + A_1 B_1(\overline{T_1}) \\ B_1(T_2) = B_1(T_s) E_2 (1-\alpha) + B_1(\overline{T_2}) A_2 \end{cases} \tag{4}$$

where subscripts 1 and 2 indicate the split window channels, centred at the lower (taken as reference) and higher wavelength, $\overline{T_1}$ and $\overline{T_2}$ are the atmospheric brightness temperatures in the two thermal channels, T_2 is the corresponding brightness temperature of I_2 and $B_i(\overline{T_i}) \equiv \overline{B_i}$ with $i=1, 2$. In equation (4), α is a shifting correcting term whose origin has been discussed in detail by Ulivieri and Cannizaro (1985a).

If the linearized Planck function around T_1 is used (Ulivieri *et al.* 1994), the corresponding brightness temperature equation yields:

$$T_s = T_1 + \beta(a_1 - 1)T_1 + a_2(T_1 - T_2) + a_3(T_s - T_{air}) \tag{5}$$

where coefficients a_j ($j=1, 2, 3$) are functions of the surface spectral emittances, the atmospheric water vapour content and the temperature profile of the atmosphere; their expressions are reported elsewhere (Ulivieri *et al.* 1994). T_{air} is the standard 2 m height air temperature, which can differ more or less significantly from T_s, depending on the nature of the surface and on the climatological conditions. In the SWT T_{air} is assumed to be equal to T_s. β, which does not vary greatly over temperature and spectral ranges of interest, is a term resulting from linearization and is given by:

$$\beta = \frac{T_1}{C_2 \nu_1} [\exp(C_2 \nu_1 / T_1) - 1] \Big/ \exp(C_2 \nu_1 / T_1) \tag{6}$$

Figure 2 shows the weak dependence of β on typical scene temperatures for the 700–1000 cm^{-1} atmospheric window together with the results obtained by accurate simulations of MODIS measurements. The simulations for the atmospheric effects in this work have been performed using the PcLnWin software package. It allows the prediction of atmospheric transmittance and radiance at high spectral resolution, as the atmospheric calculations are based on the Fast Atmospheric Signature Code (FASCODE; Clough *et al.* 1986) and the high-resolution transmission molecular absorption (HITRAN; Rothman *et al.* 1992) database. The standard built-in atmospheric profiles in FASCODE were used, together with the atmospheric conditions obtained by periodic radiosounding (once a week) performed at the Broglio Space Centre (BSC) in Malindi, Kenya. The coefficients a_j were computed for a range of water vapour content between 0.4 and 5.4 $g\,cm^{-2}$ (figure 3) for the MODIS bands 31 and 32. It can be seen that a_2 is more sensitive to the surface emittance effect than a_1 and a_3. Analogously, a_2 and, to a lesser degree, a_3 are significantly influenced by water vapour absorption. Regressive relationships

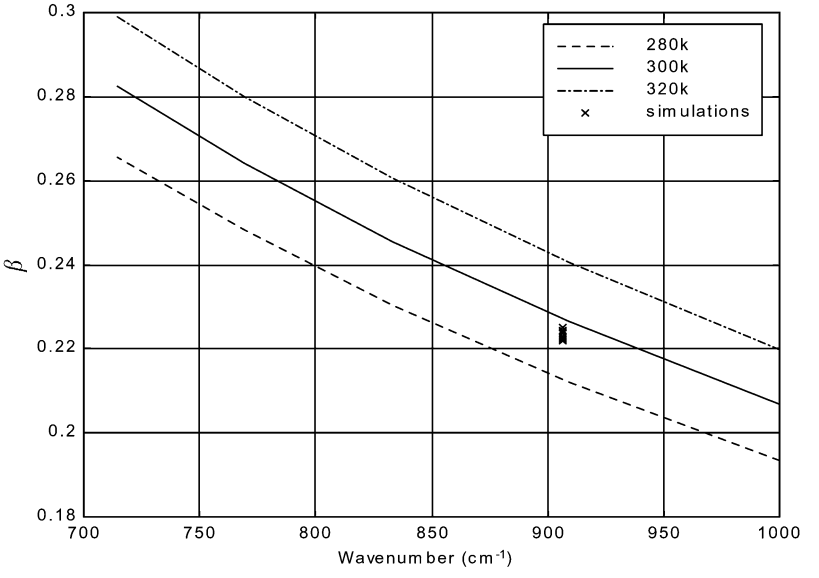

Figure 2. The β term for the 700–1000 cm^{-1} atmospheric window for typical values of scene temperatures and the MODIS simulated results.

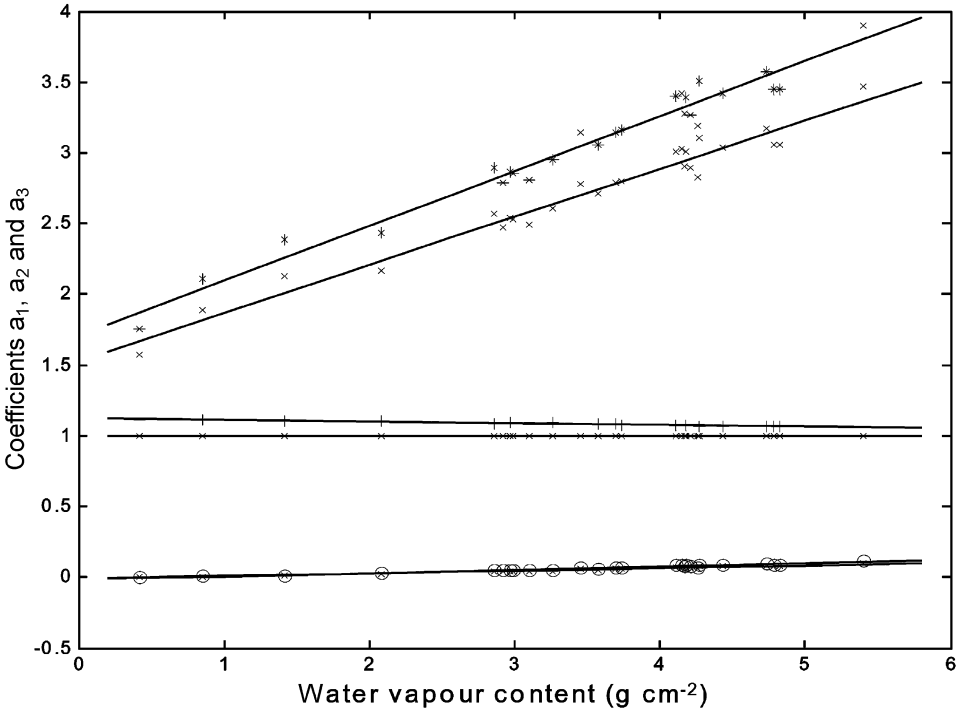

Figure 3. Coefficients of equation (5) *versus* total water vapour content for two values of mean surface emittance: $\bar{\varepsilon}=0.9(+)a_1$, $(*)a_2$, $(o)a_3$; $\bar{\varepsilon}=1(\times)a_{1,2,3}$.

for the two values of mean surface emittance are respectively:

$$\begin{cases} a'_2(\overline{\varepsilon}=1)=0.34w+1.53 \\ a'_3(\overline{\varepsilon}=1)=0.02w-0.01 \\ a'_2(\overline{\varepsilon}=0.9)=0.39w+1.71 \\ a'_3(\overline{\varepsilon}=0.9)=0.023w-0.01 \end{cases} \tag{7}$$

For $\varepsilon_1=\varepsilon_2=\overline{\varepsilon}=1$ and $T_s\cong T_{air}$ the first and the third corrective terms of equation (5) are zero; the resulting SWT algorithm is analogous to that proposed by most authors. They assume a'_2 as a constant over a wide range of w; it is evident from equation (7) that this approximation may cause a significant relative error on a'_2. Furthermore, Ulivieri (1984) showed how the a'_2 values proposed in the SWT approaches give an overestimation of the water vapour effect, which compensates for the small surface emittance effect of water bodies.

3. Assessments of the effects

In equation (5) the difference between the surface and the 2 m height air temperature reflects in the retrieved temperature through the coefficient a_3. This effect, according to the surface condition, ranges from a few tenths of a Kelvin on a water body (T_s–T_{air}=2–3 K, corresponding to 10% of the total error in the retrieved temperature) to 1 K on insulated bare soil (T_S–T_{air}=10–20 K, corresponding to 25% of the total error in the retrieved temperature) (Ulivieri and Cannizaro 1985b).

For the sake of simplicity, T_s can be assumed equal to T_{air}, the corresponding corrective term being almost independent of the other two. Then, if T'_s is the retrieved surface temperature for $\varepsilon_1=\varepsilon_2=1$, equation (5) reduces to:

$$T'_s=T_1+a'_2(T_1-T_2) \tag{8}$$

and the surface emittance effect can be evaluated by:

$$T_s-T'_s=\beta(a_1-1)T_1+(a_2-a'_2)(T_1-T_2) \tag{9}$$

Given $\delta\varepsilon=\varepsilon_1-\varepsilon_2$ and $\varepsilon_1+\varepsilon_2=2\overline{\varepsilon}$, then:

$$T_s=T'_s+H_1(1-\overline{\varepsilon})+H_2\delta\varepsilon+H_3\left[(1-\overline{\varepsilon})^2-(0.5\delta\varepsilon)^2\right] \tag{10}$$

where:

$$H_1=\frac{G_1}{D},\ H_2=\frac{G_2}{D},\ H_3=\frac{G_3}{D}$$

$$\begin{aligned}
G_1=&-\beta\left[A'_2E'_1(A'_1Z_1-1)c+A'_1E'_2(1-A'_2Z_2)\right]T_1\\
&-a'_2\left\{A'_2\left[E'_2Z_2-E'_1(1+Z_1E'_1)\right]c+A'_1E'_2(1-A'_2Z_2)\right\}(T_1-T_2)\\
G_2=&\,0.5\left\{\beta\left[A'_2E'_1(A'_1Z_1-1)c-A'_1E'_2(1-A'_2Z_2)\right]T_1\right.\\
&\left.+a'_2\left[A'_2\left(-E'_2Z_2-E'_1(1+Z_1E'_1)\right)c-A'_1E'_2(1-A'_2Z_2)\right](T_1-T_2)\right\}\\
G_3=&-\beta\left\{E'_1E'_2\left[A'_2Z_2(A'_1Z_1-1)c+A'_1Z_1(1-A'_2Z_2)\right]\right\}T_1\\
&-a'_2\left\{E'_1E'_2\left[A'_2Z_2(A'_1Z_1-1)c+A'_1Z_1(1-A'_2Z_2)\right]\right\}(T_1-T_2)\\
D=&\,cA'_2-A'_1+\left\{A'_2\left[E'_2Z_2-E'_1(1-A'_1Z_1)\right]c+A'_1\left[E'_2(1-A'_2Z_2)-E'_1Z_1\right]\right\}(1-\overline{\varepsilon})\\
&+0.5\left\{A'_2\left[E'_2Z_2+E'_1(1-A'_1Z_1)\right]c+A'_1\left[E'_2(1-A'_2Z_2)+E'_1Z_1\right]\right\}\delta\varepsilon\\
&+\left[A'_2E'_1E'_2Z_2(A'_1Z_1-1)c+A'_1E'_2E'_1Z_1(1-A'_2Z_2)\right]\left((1-\overline{\varepsilon})^2-(0.5\delta\varepsilon)^2\right)
\end{aligned}$$

where $E'_i=\tau_i$, $A'_i=1-\tau_i$, and c is a correlation coefficient, discussed elsewhere (Ulivieri *et al.* 1994).

3.1 *Estimation of H_1, H_2 and H_3*

Equation (10) was solved by linear regression analysis with least-square-sum fitting using the 21 sets of emissivity conditions as shown in table 1. The variations in H_1, H_2 and H_3 with water vapour content are illustrated in figure 4. It is evident how they are insignificantly influenced if the water vapour content is less than or equal to $3.0\,\mathrm{g\,cm^{-2}}$ and the following modified split-window algorithm can be adopted to retrieve the LST:

$$T_s = T'_s + 58.87(1-\bar{\varepsilon}) - 119.59\delta\varepsilon + 46.13\left[(1-\bar{\varepsilon})^2 - (0.5\delta\varepsilon)^2\right] \tag{11}$$

where $H_1=58.87$, $H_2=-119.59$ and $H_3=46.13$ are the calculated mean values of these functions and T'_s is evaluated for a calculated mean value of $a'_2=2.23$ in this water vapour range.

For water vapour content above $3.0\,\mathrm{g\,cm^{-2}}$ the following regressive relationships hold:

$$\begin{cases} H_1 = -7.61w + 82.69 \\ H_2 = 24.35w - 182.22 \\ H_3 = -4.81w + 65.12 \end{cases} \tag{12}$$

Table 1. Emissivity dataset used in the estimation of H_1, H_2 and H_3.

$\bar{\varepsilon}$	ε_1	ε_2	$(1-\bar{\varepsilon})$	$\delta\varepsilon$	$(1-\bar{\varepsilon})^2-(0.5\delta\varepsilon)^2$
0.98	0.99	0.97	0.02	0.02	0.00030000
	0.985	0.975		0.01	0.00037500
	0.9825	0.9775		0.005	0.00039375
	0.98	0.98		0.0	0.00040000
	0.9775	0.9825		−0.005	0.00039375
	0.975	0.985		−0.01	0.00037500
	0.97	0.99		−0.02	0.00030000
0.94	0.95	0.93	0.06	0.02	0.00350000
	0.945	0.935		0.01	0.00357500
	0.9425	0.9375		0.005	0.00359375
	0.94	0.94		0.0	0.00360000
	0.9375	0.9425		−0.005	0.00359375
	0.935	0.945		−0.01	0.00357500
	0.93	0.95		−0.02	0.00350000
0.9	0.91	0.89	0.10	0.02	0.00990000
	0.905	0.895		0.01	0.00997500
	0.9025	0.8975		0.005	0.00999375
	0.9	0.9		0.0	0.01000000
	0.8975	0.9025		−0.005	0.00999375
	0.895	0.905		−0.01	0.00997500
	0.89	0.91		−0.02	0.00990000

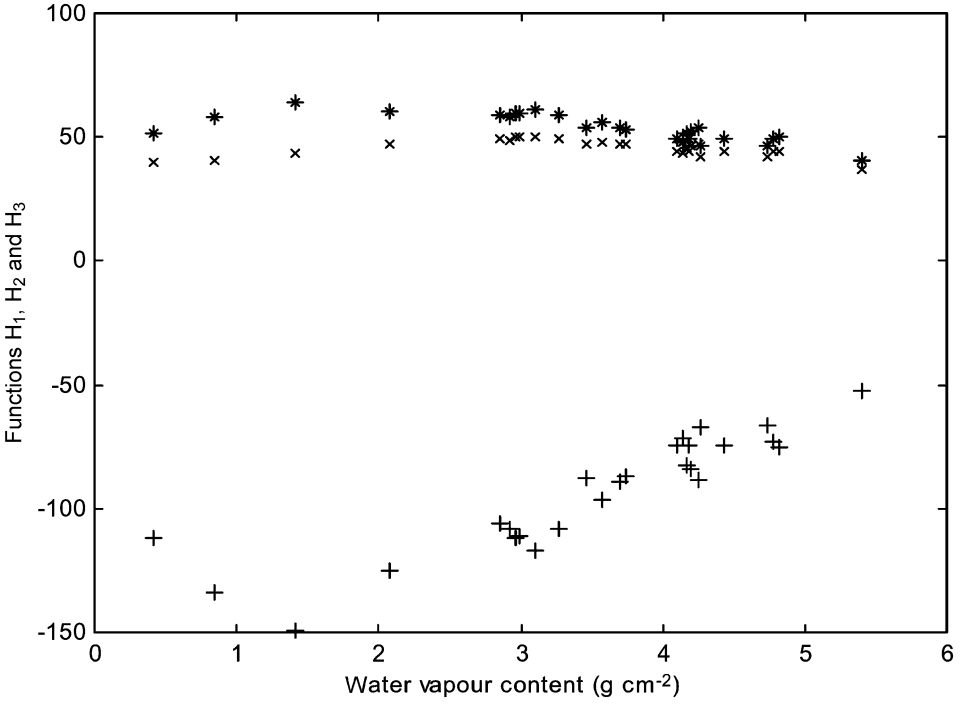

Figure 4. The H_1 (*), H_2 (+) and H_3 (×) functions *versus* water vapour content.

4. Validation results

In the MODIS LST processing, the data in MODIS Calibrated Radiance (MOD021KM) and Geolocation (MOD03) products were used together with the emissivity product from MOD11_L2 to retrieve the LST pixel by pixel. The LST validation results are given in table 2. All the *in situ* data used in the LST validation were obtained from the field campaigns conducted by the MODIS Land Discipline Group during the years 2000 and 2001 and reported in the MODIS Science Team Meeting of 18 December 2001 (http://www.icess.ucsb.edu/modis/modis-lst.html).

5. Conclusions

A simple extension of the SWT for LST determination has been set up; it is possible to express LST theoretically as a combination of the brightness temperatures in two spectrally adjacent channels, separating the atmospheric absorption and the surface emittance if the water vapour content is less than $3.0\,g\,cm^{-2}$. For any realistic value of the atmospheric water vapour content above $3.0\,g\,cm^{-2}$, the error on the temperature estimate depends strongly on the accuracy of value of the atmospheric water vapour content, and the algorithm takes advantage of the NIR/IR MODIS bands, which allow the estimation of this parameter (MOD05_L2) with a 5–10% error. In both cases the algorithm should be used in association with the emissivity information from the reflective bands to retrieve the surface temperature.

Table 2. Validation of the 1 km MODIS LST product.

Case no.	Site	Latitude Longitude	Date	Time (UTC)	CWV (cm)	*In situ* T_S (K)	$\bar{\varepsilon}$	$\delta\varepsilon$	T_{MODIS} (K)	$T_{MODIS}-T_s$ (K)
(I) In lake sites										
1	Mono Lake, CA	37.9930° N 118.9646° W	25 July 2000	19:18	2.1	296.01	0.989	0.006	295.8100	−0.2000
2	Mono Lake, CA	38.0105° N 118.9695° W	6 October 2000	19:11	1.4 (0.62)	290.17	0.989	0.006	290.6641	0.4941
3	Walker Lake, NV	38.6972° N 118.70802° W	18 October 2000	18:57	0.81 (0.95)	290.56	0.990	0.004	290.2904	−0.2696
(II) Over grassland and rice field										
4	Bridgeport, grassland	38.2202° N 119.2693° W	30 July 2000	05:57	2.4	283.24	0.988	−0.004	282.7110	−0.5290
5	Rice field, CA	39.5073° N 121.8107° W	30 July 2000	05:57	3.0	293.02	0.988	−0.004	293.0480	0.0280
6	Bridgeport, snow cover	38.2199° N 119.2683° W	12 March 2001	06:36	0.4	263.50	0.988	−0.004	264.0254	0.5254
(III) Over silt playa										
7	Silt playa in Railroad Valley, NV	38.4617° N 115.6927° W	18 July 2001	18:35	1.25 (0.86)	321.2	0.968	−0.008	320.5721	−0.6279
8	Silt playa in Railroad Valley, NV	38.4617° N 115.6926° W	20 July 2001	06:21	0.64	287.4	0.968	−0.008	287.1168	−0.2832
9	Silt playa in Railroad Valley, NV	38.4617° N 115.6926° W	21 July 2001	05:26	0.69	289.7	0.967	−0.006	289.0860	−0.6140
10	Silt playa in Railroad Valley, NV	38.4630° N 115.6930° W	21 July 2001	19:05	0.68 (0.92)	320.1	0.9680	−0.008	319.0526	−1.0474
11	Silt playa in Railroad Valley, NV	38.4630° N 115.6930° W	24 July 2001	05:57	1.01	290.7	0.9670	−0.006	290.4274	−0.2726

CWV, Column water vapour.

The LST product has been validated within 1 K, with *in situ* LSTs in 11 cases over land in the atmospheric WVC range of 0.4–3.0 $g\,cm^{-2}$. It is expected that the combined use of Terra and Aqua MODIS data will improve the LST quality significantly. In future work we expect to validate the LST products with *in situ* data from the tropical region. In this way the accuracy of the algorithm can be ascertained for this type of atmosphere, where water vapour concentrations above 3.0 $g\,cm^{-2}$ can be expected. This will allow the exploitation of the MODIS images to be acquired in future at the BSC Equatorial Station (Malindi, Kenya) for LST and SST estimates in the Central–East Africa area.

Acknowledgements

C.O.M. would like to thank Zhengming Wan, a member of the MODIS Science team and a principal investigator in NASA's Earth Observing System (EOS), for offering valuable information regarding the MODIS LST validation during an informal meeting at the First International Symposium on Recent Advances in Quantitative Remote Sensing, Valencia, Spain, 2002. Thanks also to the MODIS Science team for permission, through an email communication in 2003, to use the validation data for the comparison study.

References

BECKER, F., 1987, The impact of spectral emissivity on the measurement of land surface temperature from a satellite. *International Journal of Remote Sensing*, **8**, pp. 1509–1522.

BECKER, F. and LI, Z.L., 1990, Toward a local split window method over land surface. *International Journal of Remote Sensing*, **11**, pp. 369–393.

CLOUGH, S.E., KNEIZYS, F.X., SHETTLE, E.P. and ANDERSON, G.P., 1986, Atmospheric radiance and transmission: FASCODE2. In *Proceedings of the Sixth Conference on Atmospheric Radiation*, Williamsburg, VA (Boston, MA: American Meteorological Society), pp. 141–144.

KAHLE, A.B., MADURA, D.P. and SOHA, J.M., 1980, Middle infrared multispectral aircraft scanner data: analysis for geological applications. *Applied Optics*, **19**, pp. 2279–2290.

KERR, Y.H., LAGOUARDE, J.P. and IMBERNON, J., 1992, Accurate land surface temperature retrieval from AVHRR data with use of an improved split window algorithm. *Remote Sensing of Environment*, **41**, pp. 197–209.

KING, M.D., KAUFMAN, Y.J., MENZEL, W.P. and TANRÉ, D., 1992, Remote sensing of cloud, aerosol, and water vapour properties from Moderate Resolution Imaging Spectrometer (MODIS). *IEEE Transactions on Geoscience and Remote Sensing*, **30**, pp. 2–27.

LI, Z.L. and BECKER, F., 1993, Feasibility of land surface temperature and emissivity determination from AVHRR data. *Remote Sensing of Environment*, **43**, pp. 67–85.

MCMILLIN, L.M., 1975, Estimation of sea surface temperatures from two infrared window measurements with different absorption. *Journal of Geophysical Research*, **80**, pp. 5113–5117.

MCMILLIN, L.M., 1980, The split window algorithm for sea surface temperature derived from satellite. In *Remote Sensing of Atmospheres and Oceans*, A. Deepak (Ed.), pp. 437–455 (London: Academic Press).

OTTLE, C. and STOLL, M., 1993, Effect of atmospheric absorption and surface emissivity on the determination of land temperature from infrared satellite data. *International Journal of Remote Sensing*, **14**, pp. 2025–2037.

PRATA, A.J., 1994, Land surface temperatures derived from the advanced very high resolution radiometer and the along-track scanning radiometer. 2. Experimental results and

validation of AVHRR algorithms. *Journal of Geophysical Research*, **99**, pp. 13025–13058.

PRICE, J.C., 1984, Land surface temperature measurements from the split window channels of the NOAA-7 AVHRR. *Journal of Geophysical Research*, **79**, pp. 5039–5044.

ROTHMAN, L.S., GAMACHE, R.R., TIPPING, R.H., RINSLAND, C.P., SMITH, M.A.H., BENNER, D.C., DEVI, M.V., FLAUD, J.M., CAMY-PEYRET, C., PERRIN, A., GOLDMAN, A., MASSIE, S., BROWN, L.R. and TOTH, R.A., 1992, The HITRAN molecular database – editions of 1991 and 1992. *Journal of Quantitative Spectroscopy and Radiative Transfer*, **48**, pp. 469–507.

RUNNING, S.W., JUSTICE, C., SALOMONSON, V., HALL, D., BARKER, J., KAUFMAN, Y., STRAHLER, A., HUETE, A., MULLER, J.P., VANDERBILT, V., WAN, Z. and TEILLET, P., 1994, Terrestrial remote sensing science and algorithms planned for EOS/MODIS. *International Journal of Remote Sensing*, **15**, pp. 3587–3620.

SALISBURY, J.W. and D'ARIA, D.M., 1994, Emissivity of terrestrial materials in the 3–5 μm atmospheric window. *Remote Sensing of Environment*, **47**, pp. 345–361.

SALOMONSON, V., BARNES, W., MAYMON, P., MONTGOMERY, H. and OSTRO, H., 1989, MODIS: advanced facility instrument for studies of the Earth as a system. *IEEE Transactions on Geoscience and Remote Sensing*, **27**, pp. 145–153.

SNYDER, W. and WAN, Z., 1996, Surface temperature correction for active infrared reflectance measurements of natural materials. *Applied Optics*, **35**, pp. 2216–2220.

SNYDER, W., WAN, Z., ZHANG, Y. and FENG, Y.Z., 1997, Thermal infrared (3–14 μm) bidirectional reflectance measurements of sands and soils. *Remote Sensing of Environment*, **60**, pp. 101–109.

SOBRINO, J.A., COLL, C. and CASSELLES, V., 1991, Atmospheric corrections for land surface temperature using AVHRR channel 4 and 5. *Remote Sensing of Environment*, **38**, pp. 19–34.

ULIVIERI, C., 1984, Minimization of atmospheric water vapour and surface emittance effects on remotely sensed sea surface temperatures. *IEEE Transactions on Geoscience and Remote Sensing*, **22**, pp. 622–628.

ULIVIERI, C. and CANNIZZARO, G., 1985a, Land surface temperature retrievals from satellite measurements. *Acta Astronautica*, **12**, pp. 977–985.

ULIVIERI, C. and CANNIZZARO, G., 1985b, The influence of surface–air temperature difference on the estimate of remotely sensed surface temperatures. *Proceedings of International Conference of the Remote Sensing Society and CERMA*, London, pp. 173–178.

ULIVIERI, C., CASTRONUOVO, M.M., FRANCIONI, R. and CARDILLO, A., 1994, A split window algorithm for estimating land surface temperature from satellites. *Advances in Space Research*, **14**, pp. 59–65.

VIDAL, A., 1991, Atmospheric and emissivity correction of land surface temperature measured from satellite using ground measurements or satellite data. *International Journal of Remote Sensing*, **12**, pp. 2449–2460.

WAN, Z. and DOZIER, J., 1989, Land surface temperature measurement from space: physical principles and inverse modelling. *IEEE Transactions on Geoscience and Remote Sensing*, **27**, pp. 268–278.

WAN, Z. and DOZIER, J., 1996, A generalized split-window algorithm for retrieving land-surface temperature measurement from space. *IEEE Transactions on Geoscience and Remote Sensing*, **34**, pp. 892–905.

WAN, Z. and LI, Z.L., 1997, A physics-based algorithm for retrieving surface emissivity and temperature from EOS/MODIS data. *IEEE Transactions on Geoscience and Remote Sensing*, **35**, pp. 980–996.

WAN, Z., ZHANG, Y., ZHANG, Q. and LI, Z.L., 2002, Validation of the land surface temperature products retrieved from Terra Moderate Resolution Imaging Spectroradiometer data. *Remote Sensing of Environment*, **83**, pp. 163–180.